IEEE Access
Multidisciplinary | Rapid Review | Open Access Journal

Received November 3, 2020, accepted November 6, 2020, date of publication November 10, 2020,
date of current version November 20, 2020.

Digital Object Identifier 10.1109/ACCESS.2020.3037116

Cost-Effective Single-Inverter-Controlled Brushless Technique for Wound Rotor Synchronous Machines

SYED SABIR HUSSAIN BUKHARI[1,2], (Member, IEEE), GHULAM JAWAD SIREWAL[3], SADJAD MADANZADEH[2], (Graduate Student Member, IEEE), AND JONG-SUK RO[2]

[1]Department of Electrical Engineering, Sukkur IBA University, Sukkur 65200, Pakistan
[2]School of Electrical and Electronics Engineering, Chung-Ang University, Seoul 06974, South Korea
[3]Department of Electrical Engineering Technology, The Benazir Bhutto Shaheed University of Technology and Skill Development, Khairpur Mir's, Pakistan

Corresponding author: Jong-Suk Ro (jongsukro@gmail.com)

This work was supported in part by the Basic Science Research Program through the National Research Foundation of Korea funded by the Ministry of Education under Grant 2016R1D1A1B01008058, in part by the Human Resources Development of the Korea Institute of Energy Technology Evaluation and Planning (KETEP) funded by the Korea Government Ministry of Trade, Industry and Energy under Grant 20204030200090, and in part by the Korea Research Fellowship Program through the National Research Foundation of Korea (NRF) funded by the Ministry of Science and ICT under Grant 2019H1D3A1A01102988.

ABSTRACT This paper proposes a cost-effective brushless technique for wound rotor synchronous machines (WRSMs). The proposed technique involves a traditional current-controlled voltage source inverter that utilizes a simple hysteresis-controller-based current control scheme and supplies three-phase currents to the armature winding of the machine. The supplied armature currents inherently contain fundamental-harmonic and third-harmonic current components. These unique armature current waveforms were previously realized by using dual-inverter-controlled schemes achieved with and without thyristor switches to develop brushless WRSM topologies. The fundamental-harmonic current component is applied to develop the main stator field, whereas the third-harmonic component is employed to realize the harmonic magnetomotive force, which induces a back electromotive force (EMF) in the harmonic winding located at the rotor periphery. The induced harmonic EMF is rectified to deliver a DC current to the rotor field winding through a full-bridge diode rectifier to achieve brushless operation. The proposed cost-effective brushless technique for WRSMs is validated using 2-D finite element analysis employing JMAG-Designer 19.1 to investigate the electromagnetic and electromechanical behaviors of the machine. Furthermore, the proposed technique is employed in machine topologies with different pole/slot combinations for the armature winding to achieve better performance.

INDEX TERMS Brushless, cost-effective operation, harmonic field excitation, WRSMs.

I. INTRODUCTION

Permanent magnet (PM) machines offer numerous advantages over wound field synchronous machines (WFSMs). One such advantage is their higher efficiency due to the lack of rotor field winding and reduced copper losses [1]–[3]. Furthermore, their torque density, power density, and power factor are higher than those of WFSMs. Thus, PM machines are more suitable for applications in which high torque, efficiency, power density, and power factor are required [4].

Nevertheless, PM machines have some inherent deficiencies. One issue is the environmental pollution caused by the continuous and long-term use of rare-earth materials for manufacturing PM machines. Second, the cost of rare-earth materials has risen considerably in recent years, rendering PM machines extremely expensive. Finally, the need for a high flux weakening performance in electrical vehicle (EV) applications limits the usage of electrical machines utilizing PMs for rotor field excitation. Consequently, researchers have recently been investigating machine topologies such as WRSMs and PM-assisted synchronous reluctance machines, as these topologies either do not require a magnet for field excitation or require fewer magnets [5]–[10].

The associate editor coordinating the review of this manuscript and approving it for publication was Fabio Massaro.

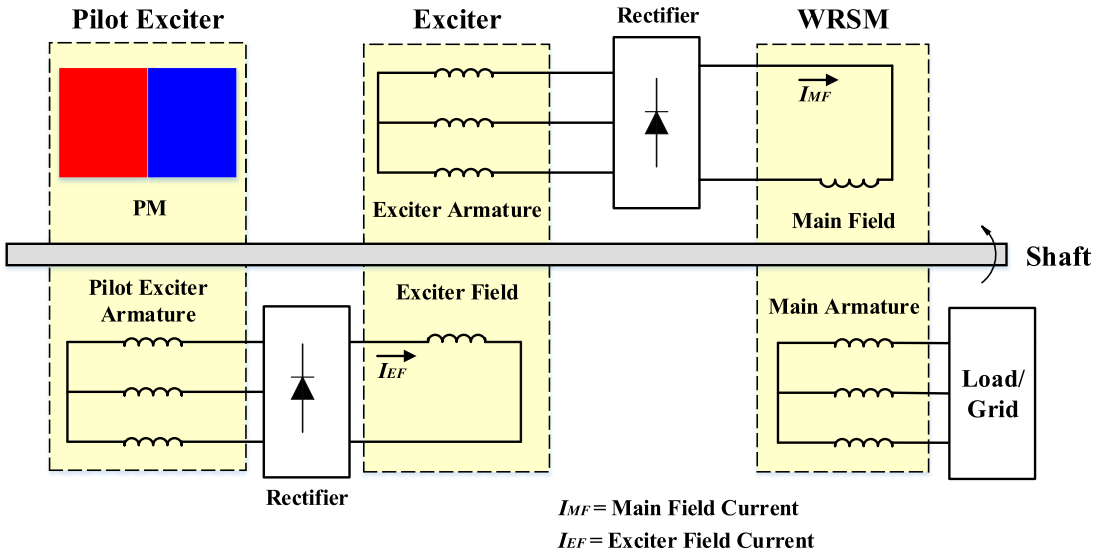

FIGURE 1. Structure of a conventional WRSM.

In a standard WRSM, the rotor field is excited by using a configuration having a combination of either brushes and slip rings or exciters and pilot exciters. In the configuration based on brushes and slip rings, the machine system faces several problems including sparking, and requires periodic maintenance. However, machines with a configuration that needs exciters and pilot exciters for rotor field excitation are bulky and expensive, which limits their adoption in small- and medium-scale applications. A typical WRSM that employs a combination of exciters and pilot exciters for rotor field excitation is presented in Fig. 1. The figure shows that the exciter and pilot exciter are two small machines mounted on the same shaft as the WRSM [11]–[15].

Thus, researchers have begun to focus on brushless topologies of WRSMs to improve their feasibility by eliminating the usage of brushes, slip rings, exciters, and pilot exciters. These brushless topologies are mainly based on a principle involving the harmonic field excitation technique [10]–[16], in which the rotor is provided a harmonic winding along with the main rotor field winding. However, the harmonics in the air gap of the machine are produced through space harmonics or time harmonics.

The authors in [17], [18] proposed a brushless WRSM topology based on a dual-inverter configuration. The inverters were linked to the two halves of the armature winding having a distinct star connection and supplying currents of different magnitudes. This arrangement caused space harmonics in the air gap around the rotor periphery. The generated harmonics were used to induce a harmonic current in the harmonic winding of the rotor, which was rectified through a diode rectifier to deliver DC current to the rotor main winding to create a rotor field. This technique was also replicated using a single inverter supplying an armature current to both halves of the stator winding. However, different numbers of turns were used in each half of the armature to maintain different magnitudes of current in the two halves. Besides the brushless operation for WRSMs, this technique adversely affected the performance of the machine due to the difference in the magnitudes of the armature currents in two different parts of the armature winding which causes higher harmonics in the machine airgap. A brushless technique for WRSM based on zero-sequence third-harmonic field excitation was proposed in [19]. This technique involved the installation of thyristor switches between the grid and the armature winding. The thyristors were operating near the zero-crossing of each phase, resulting in a considerable magnitude of zero-sequence third-harmonic current. This current was used to induce a harmonic current in the harmonic winding of the rotor, which was subsequently rectified to excite the rotor field. Although this technique achieves brushless operation for WRSMs but requires a sophisticated control strategy, complex drive circuit, and modification in machine structure to achieve the zero-crossing operation of thyristor switches. In [12], the authors proposed a brushless scheme for WRSMs established on an open winding configuration. Two inverters were linked to the two terminals of the armature winding. One inverter injected a fundamental-harmonic current, whereas the other injected a third-harmonic current. The fundamental-harmonic current was employed to develop the main stator field, whereas the third-harmonic current was used to induce a harmonic current in the harmonic winding of the rotor. This technique achieves the brushless operation for WRSMs but offers disadvantages of higher losses due to the operation of two inverters at two different frequencies, simultaneously.

Recently, a brushless topology based on a dual-inverter configuration was proposed in [20]. This topology is presented in Fig. 2(a). Here, the inverters are linked in parallel to the armature winding through thyristor switches. They deliver the armature current at a phase shift of $-180°$.

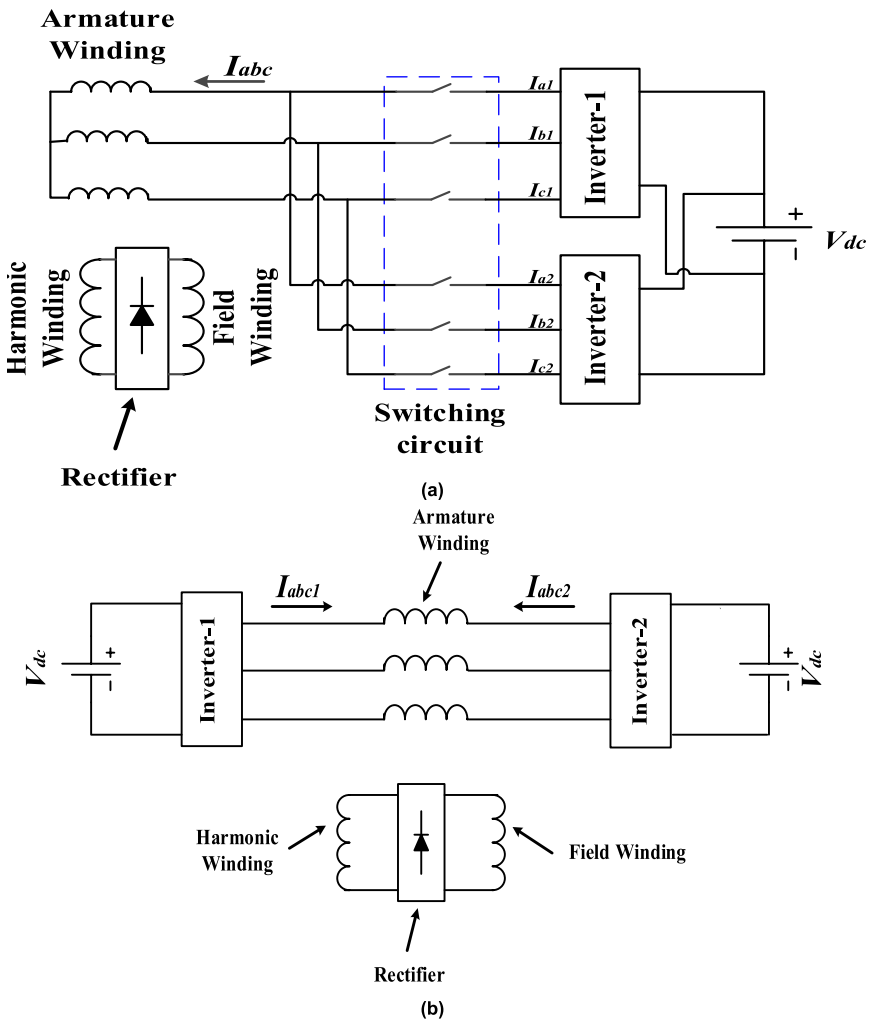

FIGURE 2. Existing dual-inverter-controlled brushless WRSM topologies, (a) with thyristors and (b) without thyristors.

The input armature currents having a composite shape inherently contain fundamental-harmonic and third-harmonic current components. The third-harmonic current component is subsequently used for the excitation of the rotor field. This technique yielded satisfactory results in terms of brushless operation and electromechanical performance. However, it involves two inverters along with thyristor switches, rendering the machine system bulky and expensive, thus limiting its implementation for medium- and small-scale power applications.

A similar composite shape of the input armature current was achieved using a dual-inverter-controlled open winding pattern technique in [21], to ensure convenient and cost-effective brushless operation for WRSMs. As presented in Fig. 2(b), this topology does not require thyristor switches, and the required shape of the input armature currents is achieved by adjusting the reference currents for each inverter. Although this technique reduces the cost, size, weight, and control complications of the previously presented brushless technique in [20], yet the usage of two inverters makes it unfavorable to be adopted for several applications.

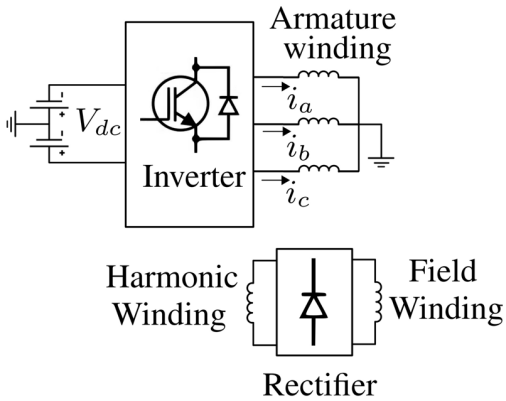

FIGURE 3. Simplified diagram of the proposed single-inverter-controlled cost-effective brushless WRSM topology.

This paper proposes a brushless technique for WRSMs using a single inverter. The composite shape of the input

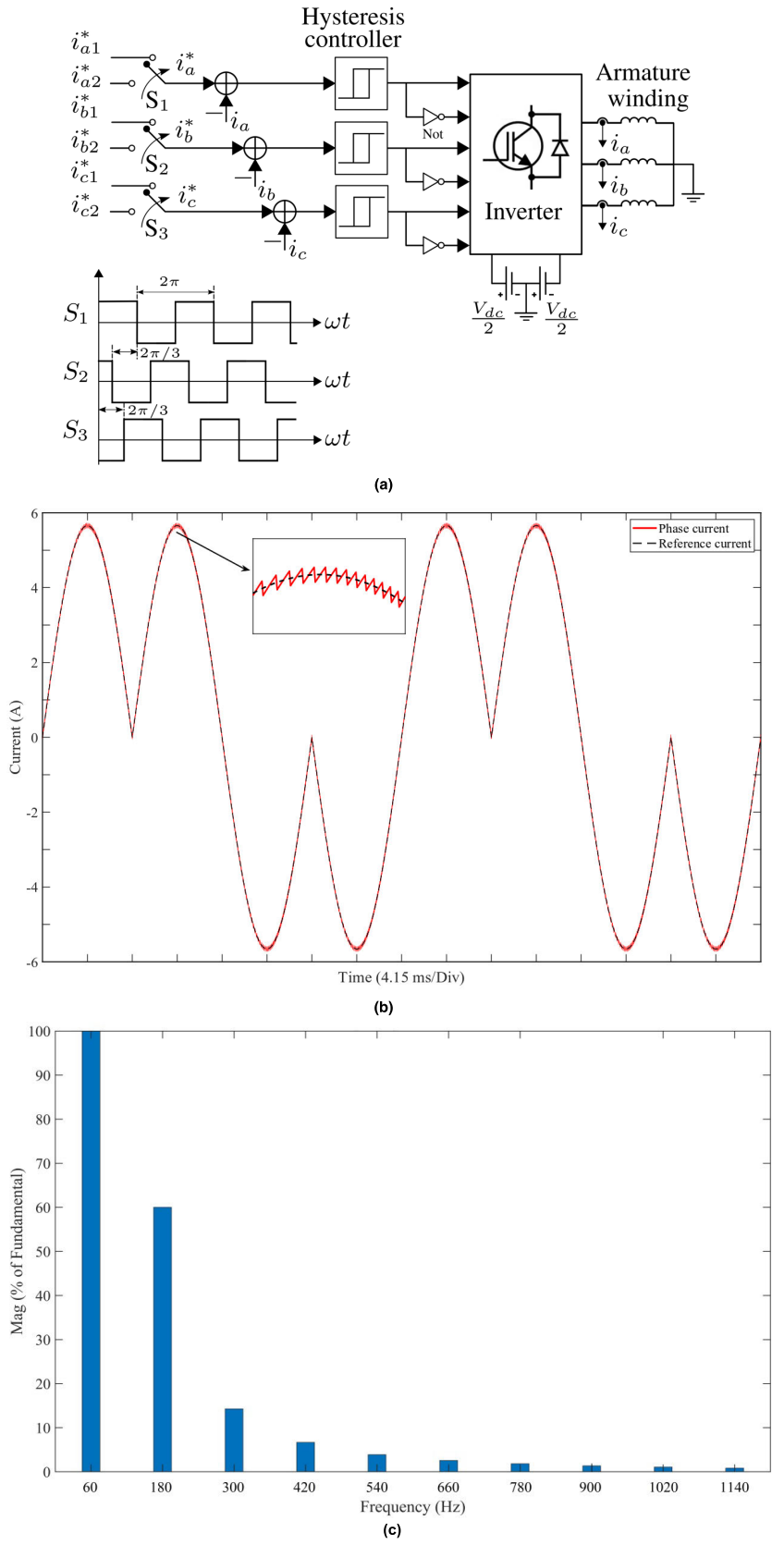

FIGURE 4. (a) Detailed illustration of the proposed inverter topology, (b) controlled output current for phase A and its (c) FFT plot.

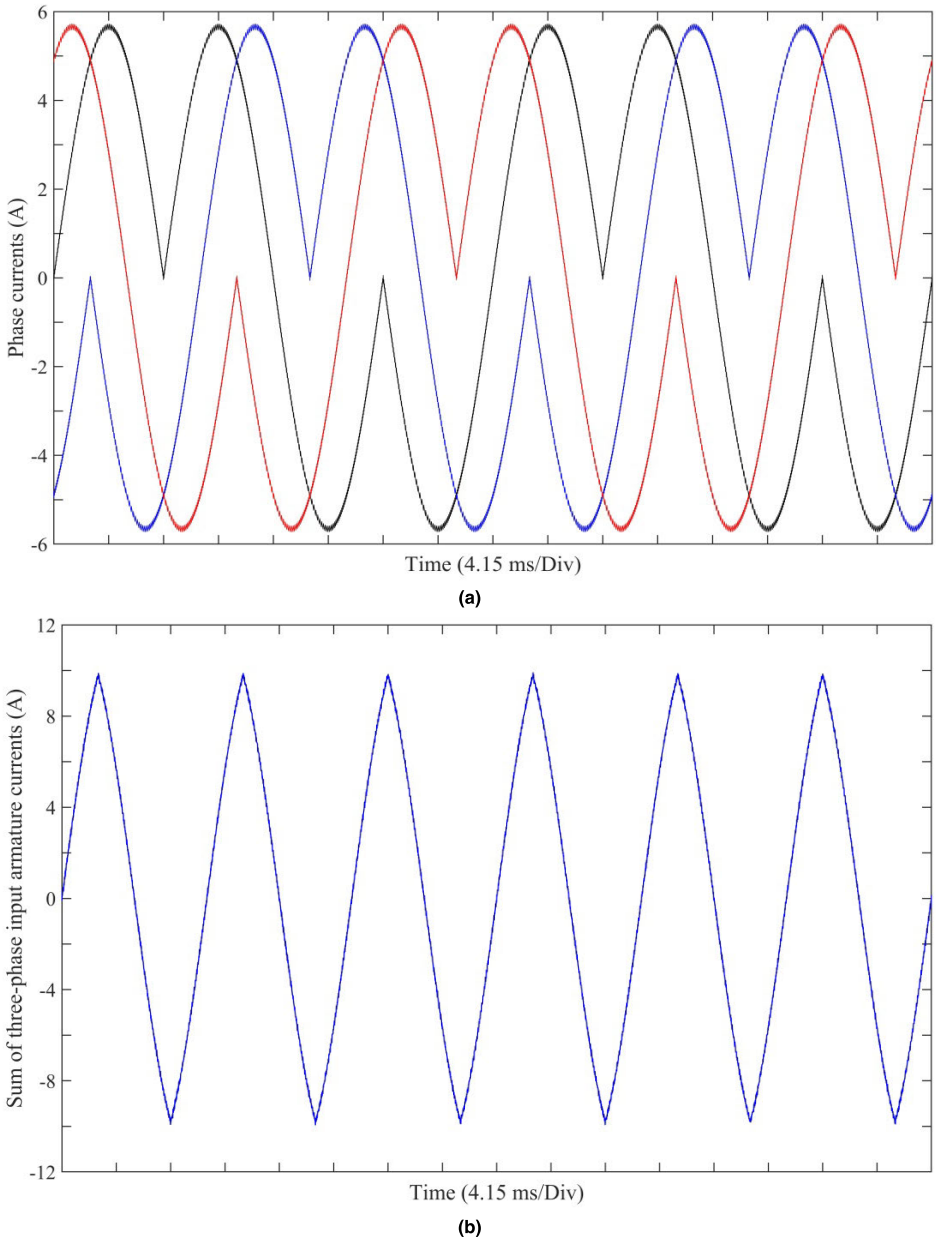

FIGURE 5. (a) Three-phase output currents of the proposed inverter topology, and (b) sum of the three-phase input armature currents.

armature currents that was previously realized using a dual-inverter operation with and without thyristor switches is achieved using a traditional current-controlled voltage source inverter that employs a simple hysteresis-controller-based current control scheme. The input armature currents inherently contain fundamental-harmonic and third-harmonic current components. Hence, the fundamental-harmonic current component is employed to produce the main stator field, whereas the third-harmonic current component is utilized to induce a harmonic current in the harmonic winding of the rotor installed at the rotor periphery. The harmonic current is then rectified using a diode rectifier to inject a DC current to the rotor field winding and achieve the brushless operation. As the proposed brushless technique is based on a traditional current-controlled voltage source inverter and uses the composite current shape, which was previously produced by using dual-inverter-controlled schemes achieved with and without thyristor switches, it proves to be cost-effective. The proposed cost-effective brushless topology for WRSMs is simply illustrated in Fig. 3. It is described in detail in the following sections.

II. PROPOSED INVERTER TOPOLOGY

The detailed illustration of the proposed inverter topology, which injects an armature current to the WRSM, is presented in Fig. 4(a). In the control part of the topology,

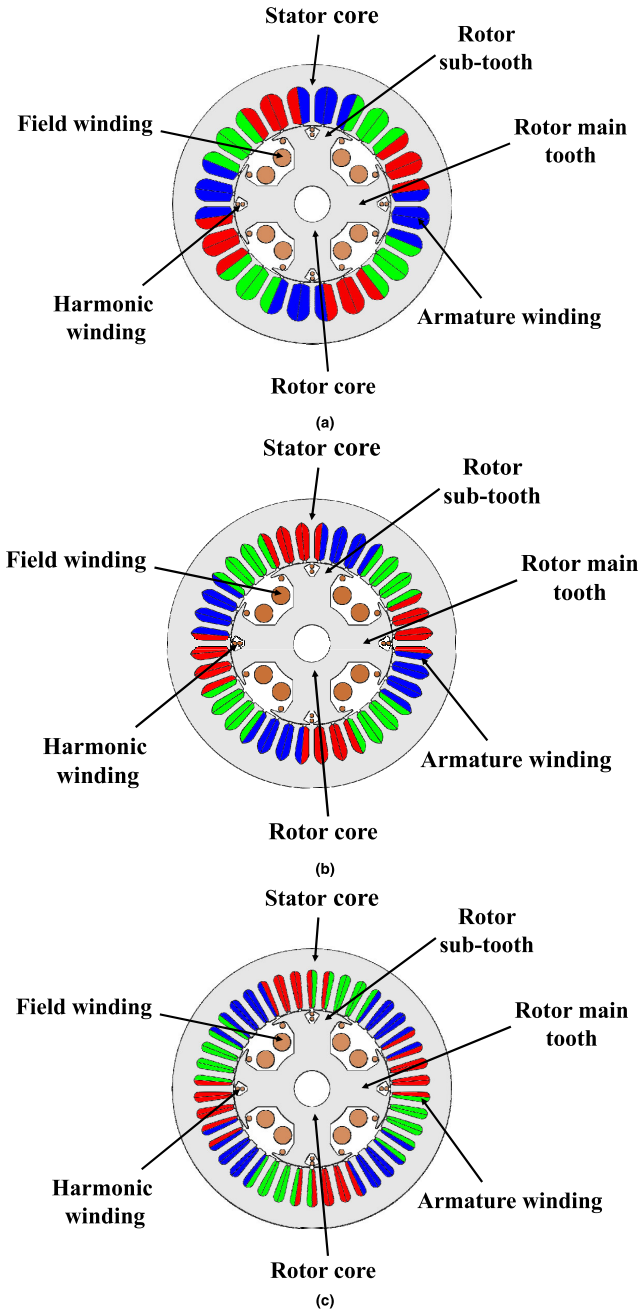

FIGURE 6. Machine models (a) Model-1, (b) Model-2, and (c) Model-3.

a typical hysteresis controller is adopted to control the phase currents with a certain hysteresis band around their references. A customary two-level voltage source inverter is employed to feed the armature currents. Input armature currents with the desired composite shape, which inherently contain fundamental-harmonic and third-harmonic current components, need to be injected. Accordingly, the proposed topology requires the inverter to have two DC sources as presented in Fig. 3 and 4(a), in which the coupled point is attached to the neutral point of the armature winding. The bandwidth of the controllers can be adjusted according to the switching potentials of the power electronic switches. Also, in Fig. 4(a) the current control is done using hysteresis control for which current references i_a^*, i_b^*, and i_c^* are produced through a selection method from the following signals as shown in this figure.

$$\begin{aligned} i_{a1}^* &= I\sin(2\omega t) \\ i_{a2}^* &= -I\sin(2\omega t) \\ i_{b1}^* &= I\sin(2\omega t - \frac{2\pi}{3}) \\ i_{b2}^* &= -I\sin(2\omega t - \frac{2\pi}{3}) \\ i_{c1}^* &= I\sin(2\omega t + \frac{2\pi}{3}) \\ i_{c2}^* &= -I\sin(2\omega t + \frac{2\pi}{3}) \end{aligned} \tag{1}$$

Fig. 4(b) illustrates the reference and controlled output currents of the inverter for phase A. The fast Fourier transform (FFT) is applied as presented in Fig. 4(c) to investigate the fundamental-harmonic and third-harmonic components of phase A of the controlled inverter output current. This analysis indicates that the third-harmonic component of the controlled output current of the inverter for phase A is approximately 60% of the fundamental-harmonic current. This magnitude of the third-harmonic current component (in percentage) depends on the shape of the input armature currents. The three-phase output currents of the proposed inverter topology are presented in Fig. 5(a). Fig. 5(b) illustrates the sum of the three-phase input armature currents, which yields a third-harmonic waveform.

The three-phase input armature current containing fundamental-harmonic and third-harmonic current components can be formulated as (1), where I_1 is the magnitude of the fundamental-harmonic of the phase currents and I_3 is the magnitude of the third-harmonic current component.

$$\left.\begin{aligned} i_a(t) &= I_1\sin(\omega t) + I_3\sin(3\omega t) \\ i_b(t) &= I_1\sin(\omega t - \frac{2\pi}{3}) + I_3\sin(3\omega t) \\ i_c(t) &= I_1\sin(\omega t + \frac{2\pi}{3}) + I_3\sin(3\omega t) \end{aligned}\right\} \tag{2}$$

Although there is a $2\pi/3$ phase difference between each one of three phases with two other ones in third harmonics. However, multiplication in 3 third harmonics has the same phase. The neutral current can be calculated as

$$I_N = i_a + i_b + i_c = 3I_3\sin(3\omega t) \tag{3}$$

and the voltage equation is as follows:

$$v_x = Ri_x + L\frac{di_x}{dt} \tag{4}$$

where $x \in \{a, b, c\}$, v_x, and i_x indicate the inverter output voltage and current for each phase, respectively. Also, R and L

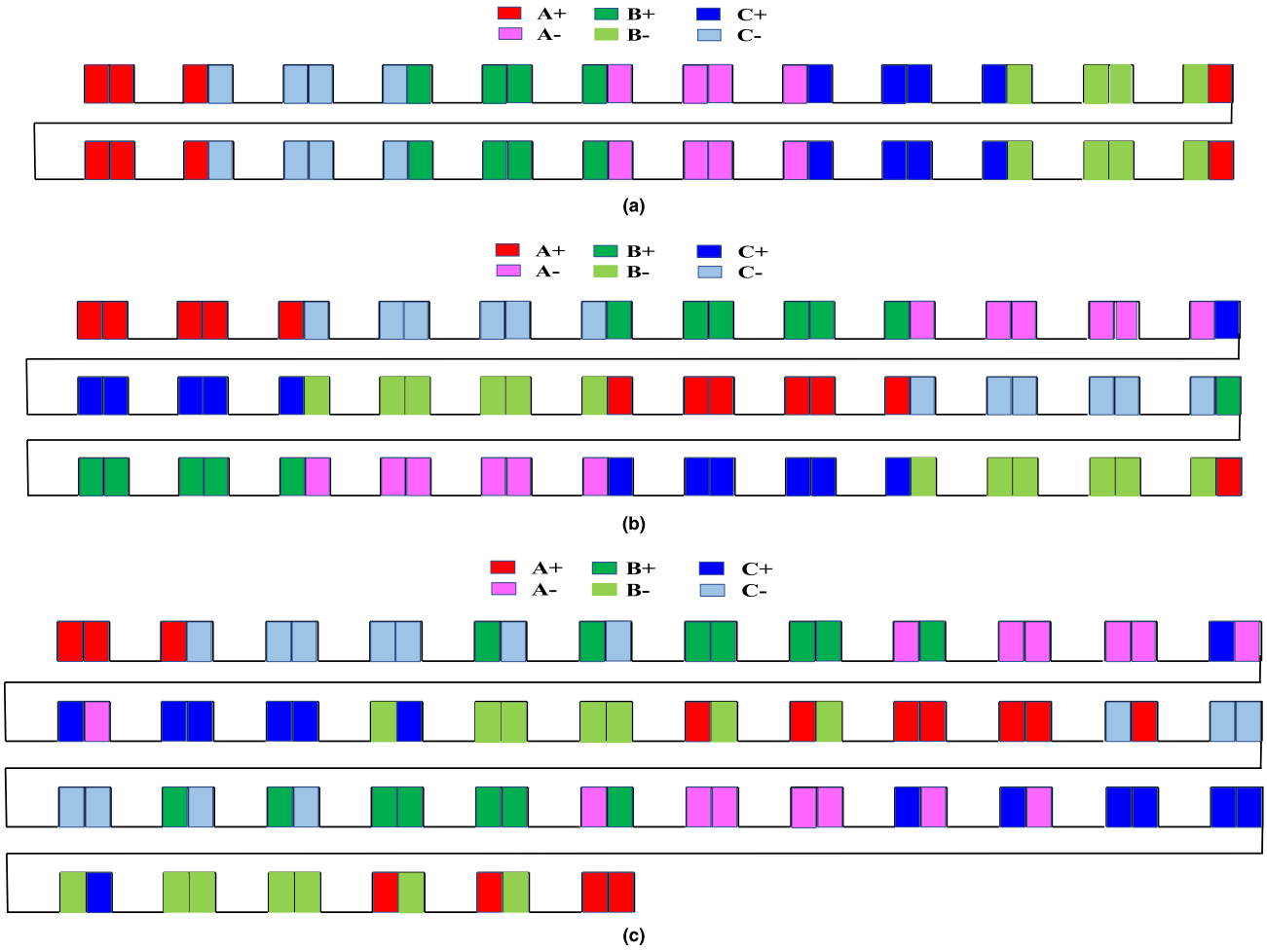

FIGURE 7. Stator winding configurations for (a) Model-1, (b) Model-2, and (c) Model-3.

TABLE 1. Winding parameters.

Attribute	Model-1	Model-2	Model-3
Number of poles/slots	4/24	4/36	4/42
Number of layers	2	2	2
Coil span	5 slots	8 slots	9 slots
Pole pitch	6 slots	9 slots	10.5 slots
Periodicities	2	2	2
Winding factor	0.933	0.945	0.932

show the resistance and inductance of the armature winding of the machine.

For the proposed method the phase a current can be given as

$$i_a(t) = \begin{cases} I\sin(2\omega t) & k\pi \le \omega t < k\pi + \dfrac{\pi}{4} \\ -I\sin(2\omega t) & k\pi + \dfrac{\pi}{4} \le \omega t < k\pi + \dfrac{3\pi}{4} \\ I\sin(2\omega t) & k\pi + \dfrac{3\pi}{4} \le \omega t < (k+1)\pi \end{cases} \tag{5}$$

where k is a member of non-negative integers. As Fig. 2 shows, $i_b(t)$ and $i_c(t)$ can be formulated through applying an initial phase for $-2\pi/3$ for $i_b(t)$ and $2\pi/3$ for $i_c(t)$. With employing the Taylor series for current waveforms, it can be seen that for example for phase a, $i_a(t)$ consists of Therefore, I_N can be calculated as follows:

$$\begin{aligned} I_N &= i_a + i_b + i_c \\ &= \begin{cases} \sin(2\omega t) + \dfrac{1}{2}\sin(2\omega t) & k\pi \le \omega t < k\pi + \dfrac{\pi}{6} \\ \sin(2\omega t) + \dfrac{\sqrt{3}}{2}\cos(2\omega t) & \\ \quad k\pi + \dfrac{\pi}{6} \le \omega t < k\pi + \dfrac{\pi}{2} & \\ -\sin(2\omega t) + \dfrac{\sqrt{3}}{2}\cos(2\omega t) & \\ \quad k\pi + \dfrac{\pi}{2} \le \omega t < k\pi + \dfrac{2\pi}{3} & \end{cases} \end{aligned} \tag{6}$$

and the voltage equation can be obtained using (4). Also, the Fourier series of (5) can be expanded to obtain I_1 and I_3 in (2) based on I in (5).

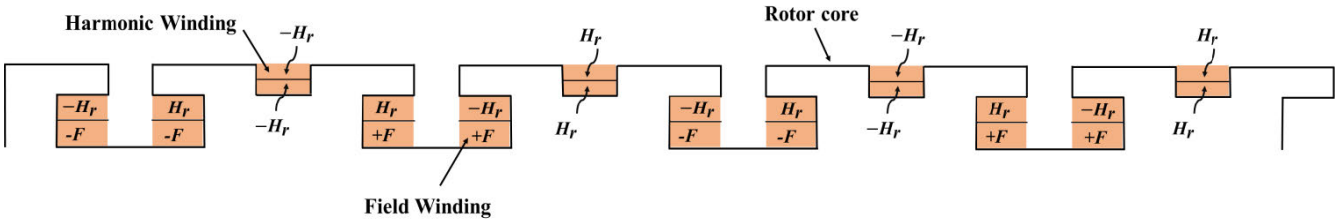

FIGURE 8. Rotor winding configuration.

TABLE 2. Specifications of the machine models.

Attribute	Model-1	Model-2	Model-3
Rated power	1.5 kW	1.5 kW	1.5 kW
Operating speed	1800 r/min	1800 r/min	1800 r/min
Stator outer/inner diameter	177/100 mm	177/100 mm	177/100 mm
Air gap	0.5 mm	0.5 mm	0.5 mm
Rotor outer diameter	99 mm	99 mm	99 mm
Machine poles/Stator slots	4/24	4/36	4/42
Shaft diameter	23 mm	23 mm	23 mm
Rotor main teeth/sub-teeth	4/8	4/8	4/8
Stator winding number of turns	20	20	20
Harmonic/field winding number of turns (for all poles)	9/150	9/150	9/150
Stack length	80 mm	80 mm	80 mm

III. MACHINE TOPOLOGY AND WORKING PRINCIPLE

Three machine models with different numbers of slots as presented in Fig. 6 are adopted to validate the proposed cost-effective brushless technique for WRSMs. Model-1 is based on a configuration with 4 poles and 24 slots. Model-2 and model-3 are constructed based on configurations with 4 poles and 36 slots, and 4 poles and 42 slots, respectively. The winding arrangements for each of the adopted models are presented in Fig. 7. However, the detailed specifications of the winding configurations employed in the investigated models are listed in Table 1.

The machine models are supplied with the input armature currents having the composite shape, which are produced through the inverter topology discussed in the previous section. These currents create a 4-pole fundamental-harmonic and 12-pole third-harmonic magnetomotive force (F) in the air gap. The created MMF is given by

$$\begin{aligned} F_a &= i_a N_\phi \sin\theta_e \\ F_b &= i_b N_\phi \sin(\theta_e - \frac{2\pi}{3}) \\ F_c &= i_c N_\phi \sin(\theta_e + \frac{2\pi}{3}) \end{aligned} \tag{7}$$

where N_ϕ indicates the number of turns per phase, and $\theta_e = \omega t + \theta_0$, ($\theta_e$ is used to denote the electrical angle whereas θ_0 indicates the initial rotor position).

The net MMF (F_{abc}) produced owing to the supplied three-phase input armature currents is given by

$$F_{abc}(\theta_e, i_{abc}) = \frac{3}{2} I_1 N_\phi \cos(\omega t - \theta_e) + I_3 N_\phi \cos 3(\omega t + \theta_e) \tag{8}$$

The aforementioned net created MMF contains the fundamental-harmonic and the third-harmonic components of the MMF. The resulting MMF expression contains third harmonic MMF component due to the inherent third-harmonic current calculated from (5). The fundamental-harmonic component of the MMF produces the main stator field, whereas the third-harmonic component of the MMF creates a pulsating field in the air gap.

The rotor of the machine is equipped with the field winding and a specially designed harmonic winding placed on the rotor teeth and sub-teeth, respectively. The pulsating third harmonic field from the air gap links with the harmonic winding due to the difference of rotor speed with reference to the air gap third harmonic flux. The flux linkage to the rotor harmonic winding is then computed as

$$\lambda_{H_r} = \frac{N_{H_r} N_\phi (\frac{3}{2} I_1 \cos(\omega t - \theta_e) + n I_3 \cos(3\omega t + 3\theta_e))}{R_g} \tag{9}$$

where N_{Hr} is the number of rotor harmonic turns and R_g is the air-gap reluctance [5].

The induced electromotive force in the rotor harmonic winding (EMF_{Hr}) of the machines is expressed by (10), where six harmonic coils are available during one electrical rotation.

$$EMF_{H_r} = 6\frac{d\lambda_{H_r}}{dt} = \frac{18 N_{H_r} N_\phi I_3 \omega \sin 3\,(2\omega t + \theta_0)}{R_g} \tag{10}$$

where λ_{Hr} indicates the flux linkages for the harmonic winding of the rotor.

The induced EMF in the harmonic winding is rectified to deliver a DC current to the rotor main field winding. The

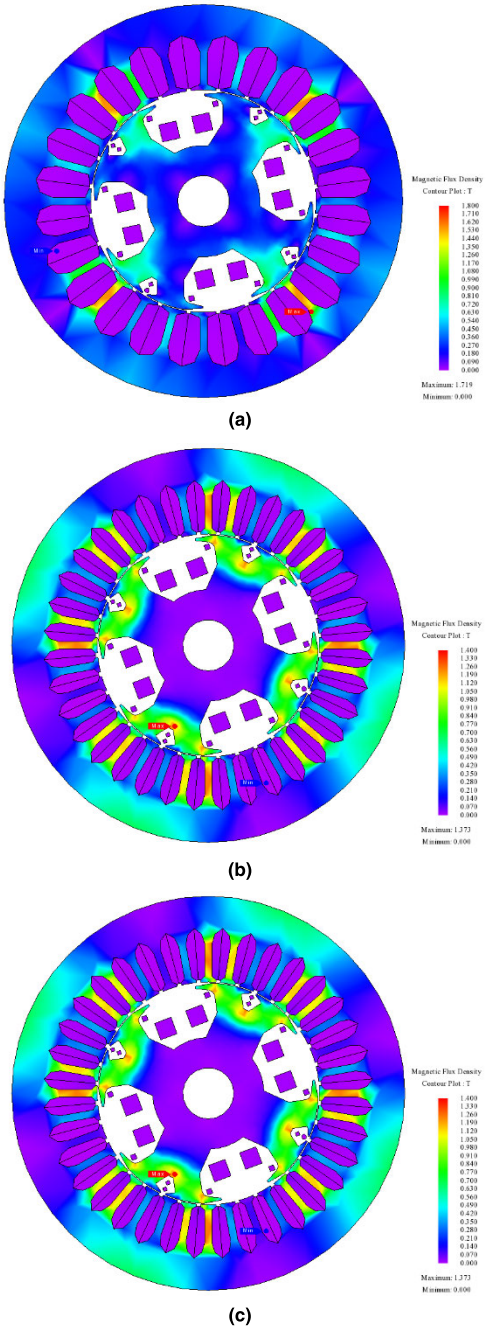

FIGURE 9. Magnetic flux density plots for (a) Model-1, (b) Model-2, and (c) Model-3.

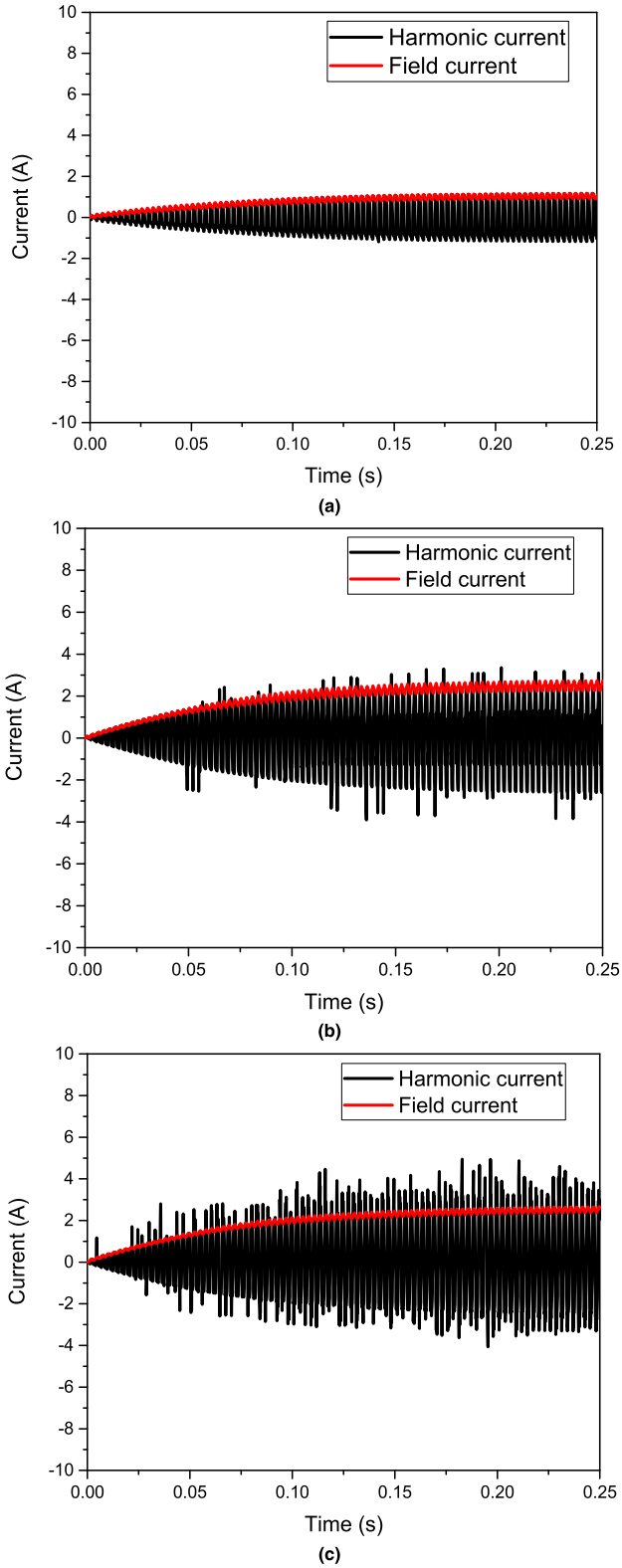

FIGURE 10. Harmonic and field currents for (a) Model-1, (b) Model-2, and (c) Model-3.

rotor field interacts with the main stator field caused by the fundamental-harmonic component of the MMF, thus producing torque. The simplified rotor structure for the adopted machine models is illustrated in Fig. 8.

IV. FINITE ELEMENT ANALYSIS

Three finite element machine models were developed to investigate the electromagnetic and electromechanical performances of the proposed cost-effective brushless technique for WRSMs. The main parameters of these machine models are considered the same for a better comparison of their performances as summarized in Table 2.

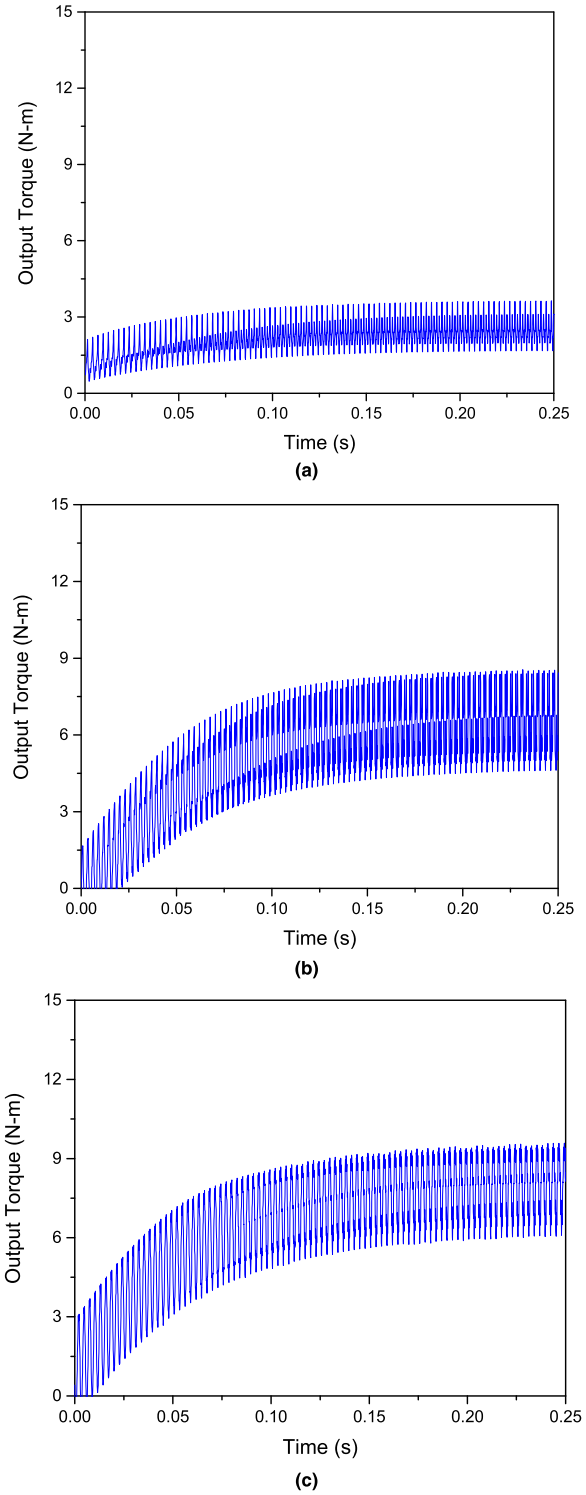

FIGURE 11. Output torque for (a) Model-1, (b) Model-2, and (c) Model-3.

The machine models operate at a constant speed of 1800 r/min. The simulations are carried out for 2s with the number of divisions equal to 21600 and a time interval of 92.5 μs.

TABLE 3. Performance comparison.

Attribute	Model-1	Model-2	Model-3
Average output torque (Nm)	2.515	6.407	8.143
Maximum output torque (Nm)	3.65	8.61	10.63
Torque ripple (%)	78.10	60.89	40.64
Efficiency (%)	89.54	91.66	92.99

The armature winding of all the investigated models denoted as the 4p24s, 4p36s, and 4p42s models, is provided with a current of 4.0 A (RMS) generated through the proposed inverter topology. As the input armature currents having the composite shape inherently contain fundamental-harmonic and third-harmonic current components, a 4-pole main stator field, and a 12-pole third-harmonic pulsating field are produced in the air gap. Fig. 9 plots the magnetic field density for the investigated machine models under these conditions. These plots reveal that the working magnetic field densities of the machines never exceed the saturation limits of 1.8 T for model-1 and 1.4 T for model-2 and model-3 respectively, during the loaded operation.

The 12-pole third-harmonic MMF induces an EMF in the harmonic winding of the rotor, which is rectified through the diode rectifier placed between the harmonic and rotor field windings. The output of the rectifier is used to excite the rotor field winding. The harmonic and field currents of the investigated machine models are presented in Fig. 10. Fig. 11 illustrates the output torque for the same machine models. This figure confirms that, under the same main parameters and operating conditions, the average torque of the 4p42s machine model is 8.143 Nm, which is 2.237 times higher than that of the 4p24s machine model and 0.27 times higher than that of the 4p36s machine model. The magnitude of the maximum torque for the 4p42s machine model is 10.63 Nm. However, its magnitude is 8.61 Nm and 3.65 Nm for 4p36s and 4p24s machine models, respectively. The torque ripple of model-3 is approximately 40.64%, which is 92.175% lower than that of model-1 and 49.82% lower than that of model-2. On the other hand, the efficiency of 4p24s, 4p36s, and 4p42s machine models is 89.54%, 91.66%, and 92.99%. The magnitudes of the average output torque, maximum torque, torque ripple, and efficiency for the investigated models are listed in Table 3. The higher magnitude of torque ripple for the investigated machine models can be improved with machine structure optimization for specific applications.

The proposed brushless WRSM topology as discussed in previous sections is based on a customary current-controlled voltage source inverter to realize a unique input armature current shape which was previously achieved using dual-inverter-controlled WRSM topologies. A comparison of these existing brushless topologies with the proposed cost-effective topology is presented in Table. 4.

TABLE 4. Comparison of the existing and proposed brushless WRSM topologies.

Topology	Cost	Weight	Size
Dual-inverter-controlled topology with thyristors	Highest	Highest	Largest
Dual-inverter-controlled topology without thyristors	Higher	Higher	Larger
Proposed single-inverter-controlled topology	Low	Low	Small

V. CONCLUSION

A cost-effective brushless technique for WRSMs was proposed in this paper. A single customary inverter that employs a simple hysteresis current controller was used to inject a composite input armature current that inherently contains fundamental-harmonic and third-harmonic components. The fundamental-harmonic current was used to develop the main stator field, whereas the third-harmonic current was used to induce a harmonic current in the harmonic winding of the rotor, which was rectified to inject a DC current to the field winding to achieve the brushless operation. Finite element analysis was presented to confirm the proposed technique and achieve the output torque for three machine models having different numbers of pole/slot combinations. From the results, it was concluded that the average output torque of the 4p42s machine model is 1.736 Nm higher than 4p36s and 5.628 Nm higher than 4p24s machine models. The maximum output torque of the 4p42s machine model is 2.02 Nm higher than 4p36s and 6.98 Nm higher than 4p24s machine models. Besides, the torque ripple for the 4p42s machine model is 20.025% lower than 4p36s and 29.46% lower than 4p24s machine models. Furthermore, the efficiency of the 4p42s machine model is 1.33% higher than 4p36s and 3.45% higher than 4p24s machine models.

The proposed brushless technique is simple and cost-effective, as it is based on a single inverter and does not require any additional hardware and sophisticated control strategy compared to the available dual-inverter-controlled brushless WRSM topologies operating to achieve the same input armature current shape. This decreases the size and weight of the machine systems as well. Given the advantages of the proposed topology, a conventional machine can be replaced with it for the cheaper production without compromising the performance of the application. Hence it can be used in many small-scale three-phase industrial drives.

REFERENCES

[1] S. Khan, S. S. H. Bukhari, and J.-S. Ro, "Design and analysis of a 4-kW two-stack coreless axial flux permanent magnet synchronous machine for low-speed applications," *IEEE Access*, vol. 7, pp. 173848–173854, 2019.
[2] B. J. Chalmers, R. M. Magureanu, and J. Hindmarsh, "General principle for brushless synchronous machines and its application in an inverter-fed drive," *Proc. IEE*, vol. 119, no. 11, pp. 1641–1642, Nov. 1972.
[3] B. J. Chalmers and R. M. Magureanu, "Synchronous electrical machines," U.S.Patent 3 757 182, Sep. 4, 1973.
[4] K. Inoue, H. Yamashita, E. Nakamae, and T. Fujikawa, "A brushless self-exciting three-phase synchronous generator utilizing the 5th-space harmonic component of magneto motive force through armature currents," *IEEE Trans. Energy Convers.*, vol. 7, no. 3, pp. 517–524, Sep. 1992.
[5] L. Sun, X. Gao, F. Yao, Q. An, and T. Lipo, "A new type of harmonic current excited brushless synchronous machine based on an open winding pattern," in *Proc. IEEE Energy Convers. Congr. Expo. (ECCE)*, Pittsburgh, PA, USA, Sep. 2014, pp. 2366–2373.
[6] F. Yao, Q. An, L. Sun, and T. A. Lipo, "Performance investigation of a brushless synchronous machine with additional harmonic field windings," *IEEE Trans. Ind. Electron.*, vol. 63, no. 11, pp. 6756–6766, Nov. 2016.
[7] M. Ayub, S. Atiq, Q. Ali, A. Hussain, and B.-I. Kwon, "Dual-mode wound rotor synchronous machine for variable speed applications," *IEEE Access*, vol. 8, pp. 115812–115822, 2020.
[8] M. Ayub, A. Hussain, G. Jawad, and B.-I. Kwon, "Brushless operation of a wound-field synchronous machine using a novel winding scheme," *IEEE Trans. Magn.*, vol. 55, no. 6, Jun. 2019, Art. no. 8201104.
[9] A. Hussain, S. Atiq, and B.-I. Kwon, "Consequent-pole hybrid brushless wound-rotor synchronous machine," *IEEE Trans. Magn.*, vol. 54, no. 11, Nov. 2018, Art. no. 8206205.
[10] F. Yao, Q. An, X. Gao, L. Sun, and T. A. Lipo, "Principle of operation and performance of a synchronous machine employing a new harmonic excitation scheme," *IEEE Trans. Ind. Appl.*, vol. 51, no. 5, pp. 3890–3898, Sep. 2015.
[11] M. Ayub, S. S. H. Bukhari, G. Jawad, and B.-I. Kwon, "Brushless wound field synchronous machine with third-harmonic field excitation using a single inverter," *Electr. Eng.*, vol. 101, no. 1, pp. 165–173, Apr. 2019.
[12] Q. An, X. Gao, F. Yao, L. Sun, and T. Lipo, "The structure optimization of novel harmonic current excited brushless synchronous machines based on open winding pattern," in *Proc. IEEE Energy Conver. Cong. Expo. (ECCE)*, Pittsburgh, PA, USA, 2014, pp. 1754–1761.
[13] M. Ayub, G. Jawad, and B.-I. Kwon, "Consequent-pole hybrid excitation brushless wound field synchronous machine with fractional slot concentrated winding," *IEEE Trans. Magn.*, vol. 55, no. 7, pp. 1–5, Jul. 2019, Art. no. 8203805.
[14] M. Ayub, S. Atiq, G. J. Sirewal, and B.-I. Kwon, "Fault-tolerant operation of wound field synchronous machine using coil switching," *IEEE Access*, vol. 7, pp. 67130–67138, 2019.
[15] F. Yao, Q. An, L. Sun, M. S. Illindala, and T. A. Lipo, "Optimization design of stator harmonic windings in brushless synchronous machine excited with double-harmonic-windings," in *Proc. Int. Energy Sustainability Conf. (IESC)*, Oct. 2017, pp. 1–6.
[16] J. C. Chapman, *Electric Machinery Fundamentals*, 5th ed. New Delhi, India: McGraw-Hill, 2017.
[17] Q. Ali, T. A. Lipo, and B.-I. Kwon, "Design and analysis of a novel brushless wound rotor synchronous machine," *IEEE Trans. Magn.*, vol. 51, no. 11, Nov. 2015, Art. no. 8109804.
[18] Q. Ali, S. S. H. Bukhari, and S. Atiq, "Variable-speed, sub-harmonically excited BL-WRSM avoiding unbalanced radial force," *Electr. Eng.*, vol. 101, no. 1, pp. 251–257, Apr. 2019.
[19] G. Jawad, Q. Ali, T. A. Lipo, and B.-I. Kwon, "Novel brushless wound rotor synchronous machine with zero-sequence third-harmonic field excitation," *IEEE Trans. Magn.*, vol. 52, no. 7, Jul. 2016, Art. no. 8106104.
[20] M. Ayub, G. J. Sirewal, S. S. H. Bukhari, and B.-I. Kwon, "Brushless wound rotor synchronous machine with third-harmonic field excitation," *Electr. Eng.*, vol. 102, no. 1, pp. 259–265, Mar. 2020.
[21] S. S. H. Bukhari, G. J. Sirewal, F. A. Chachar, and J.-S. Ro, "Dual-Inverter-Controlled brushless operation of wound rotor synchronous machines based on an open-winding pattern," *Energies*, vol. 13, no. 9, p. 2205, May 2020.

SYED SABIR HUSSAIN BUKHARI (Member, IEEE) received the B.E. degree in electrical engineering from the Mehran University of Engineering and Technology, Jamshoro, Pakistan, in 2009, and the Ph.D. degree from the Department of Electronic Systems Engineering, Hanyang University, South Korea, in 2017. He joined Sukkur IBA University, in December 2016, as an Assistant Professor. He is currently working as a Research Professor with Chung-Ang University, Seoul, South Korea, under Korean Research Fellowship (KRF) program. His main research interests include electric machine design, power quality, and drive controls.

GHULAM JAWAD SIREWAL was born in Tando Allahyar, Sindh, Pakistan, in 1988. He received the B.E. degree in electrical engineering and the P.G.D. degree in electrical power engineering from the Mehran University of Engineering and Technology, Jamshoro, Pakistan, in 2011 and 2012, respectively, and the Ph.D. degree from the Department of Electrical and Electronic Engineering, Hanyang University, Ansan, South Korea, in 2020. He is currently an Assistant Professor with the Department of Electrical Engineering Technology, The Benazir Bhutto Shaheed University of Technology and Skill Development, Khairpur Mir's, Sindh, Pakistan. His research interest includes electric machine design and control.

SADJAD MADANZADEH (Graduate Student Member, IEEE) received the B.S. degree in electrical engineering from the University of Zanjan, Zanjan, Iran, in 2010, and the M.S. degree in electrical engineering from the K. N. Toosi University of Technology, Tehran, Iran, in 2013. He is currently a Researcher with Chung-Ang University, Seoul, South Korea. His research interests include electric drives control, electrical machine design, and power electronics.

JONG-SUK RO received the B.S. degree in mechanical engineering from Hanyang University, Seoul, South Korea, in 2001, and the Ph.D. degree in electrical engineering from Seoul National University (SNU), Seoul, in 2008.

He conducted research at the Research and Development Center, Samsung Electronics, as a Senior Engineer, from 2008 to 2012. From 2012 to 2013, he was with the Brain Korea 21 Information Technology of SNU, as a Postdoctoral Fellow. He also conducted research at the Electrical Energy Conversion System Research Division, Korea Electrical Engineering & Science Research Institute, as a Researcher, in 2013. From 2013 to 2016, he worked with the Brain Korea 21 Plus, SNU, as a BK Assistant Professor. In 2014, he was with the University of Bath, Bath, U.K. He is currently an Associate Professor with the School of Electrical and Electronics Engineering, Chung-Ang University, Seoul. His research interests include the analysis and optimal design of next-generation electrical machines using smart materials, such as electromagnet, piezoelectric, and magnetic shape memory alloy.